crystals

MDPI

Article

Al-Si@Al(OH)$_3$ Nanosheets Composite for Enhanced Efficient Strategy to Synthesize Al-Si@Al$_2$O$_3$ Core-Shell Structure

Yuhui Lin, Panyu Chen, Ying Wang and Chengdong Li *

College of Materials Science and Engineering, Qingdao University of Science and Technology,
Qingdao 266042, China
* Correspondence: lichengdong@qust.edu.cn

Abstract: Owing to the combined advantages of Al-Si alloy and Al$_2$O$_3$, Al-Si@Al$_2$O$_3$ is widely utilized as a heat storage material, catalyst carrier, and water adsorption host. Hence, the preparation of Al-Si@Al$_2$O$_3$ and corresponding precursors is of utmost significance. Herein, an Al-Si@Al(OH)$_3$ precursor is investigated, and Al(OH)$_3$ nanosheets are in situ formed on the surface of Al1-xSix, where x = 0,10, 0,20, and 0,30 in the presence of water. The influence of the Si content, diameter of Al-Si particles, and heating parameters on the morphology and thickness of the Al(OH)$_3$ nanosheets is systematically explored using X-ray diffraction, electron microscopy, Fourier transform infrared spectroscopy, and N$_2$ adsorption/desorption isotherms. The growth mechanism of Al(OH)$_3$ nanosheets is revealed, and a pathway to obtain Al-Si@Al$_2$O$_3$ nanosheets with the desired structure and thickness is demonstrated.

Keywords: surfaces; nanocomposite; microstructure; Al-Si particles; Al(OH)$_3$ nanosheets

check for updates

Citation: Lin, Y.; Chen, P.; Wang, Y.; Li, C. Al-Si@Al(OH)$_3$ Nanosheets Composite for Enhanced Efficient Strategy to Synthesize Al-Si@Al$_2$O$_3$ Core-Shell Structure. *Crystals* **2022**, *12*, 1137. https://doi.org/10.3390/cryst12081137

Academic Editor: Cyril Cayron

Received: 24 July 2022
Accepted: 11 August 2022
Published: 12 August 2022

1. Introduction

The term core-shell structure first appeared in nanotechnology and extended to various subject areas. The core-shell structure is a two-component system that combines both components' respective characteristics to meet the intensive requirements of the advanced applications [1]. Recently, core-shell structured materials have garnered significant research attention due to their comprehensive properties and designability as photocatalysts [2], thermal storage material [3], and adsorption material [4]. Different methods can be used to obtain the core–shell structures, including the hydrothermal method [5–7], sol–gel process [8–10], arc discharge method [11–13], and the one pot approach [14–16].

The Al-Si alloy is a cost-effective, highly conductive, and thermally stable candidate, which can easily form a core-shell structure with an Al-Si alloy as a core and Al$_2$O$_3$ as a shell [17]. The low specific area and high-temperature corrosion of the Al-Si alloy, however, greatly limit the practical applications. Hence, alumina (Al$_2$O$_3$) is usually coated on the surface of the Al-Si alloy due to its high specific area, chemical inertness, and thermal stability [18]. For instance, Han et al. [19] reported a facile hydrothermal process to synthesize γ-Al$_2$O$_3$ on the surface of Al-40Si powder, revealing the growth mechanism of AlOOH nanoflakes on the surface. Dai et al. [20] prepared Al-Si@Al$_2$O$_3$ by the hydrothermal method and further investigated the effect of size and aluminum content in Al-Si powder on the catalytic performance of Pb/Al-Si@Al$_2$O$_3$. The results indicated that the Pb/Al-Si@Al$_2$O$_3$ catalyst possessed optimal hydrogenation performance when the size and aluminum content were 5 µm and 88%, respectively.

Al-Si powder, with different amounts of Si, exhibits different morphologies [21–23]. The eutectic Si can be observed when the Si content in Al-Si powder is close to 12.6 at. %. Eutectic Si and primary Si coexist in Al-Si powder when the Si content is higher than 12.6 at. %. Meanwhile, the primary Si became more irregular and larger with the increase in Si content. These studies demonstrated that AlOOH nucleated at the Si substrate; however, the influence of Si morphology on the nucleation of hydrated alumina has been neglected in these studies.

Herein, Al-Si powder, with different amounts of Si, was selected to explore the impact of Si morphology on $Al(OH)_3$ nucleation. Research has shown that the morphology can be maintained, while the phase change rose from boehmite to γ-Al_2O_3 [4]. Hence, instead of calcination temperature, the structure of Al_2O_3 is mainly influenced by the Si content. The silicon morphology of Al-Si powders had different characteristic in diverse particle sizes, which resulted from the solidification rate [24]; the particle size was also a significant research factor. Furthermore, $Al(OH)_3$ was prepared on the surface of Al-Si particles using the hydrothermal and water bath methods. In addition, the influence of reaction time, Si content, and particle size on the structure of Al-Si@$Al(OH)_3$ precursor is discussed, and the mechanism of the in situ formation of $Al(OH)_3$ nanoflakes is investigated.

2. Experiments

Al-Si powder was treated using deionized water at 80 °C for 3 h under the hydrothermal method, followed by centrifugation, washing with absolute alcohol thrice, and drying at 50 °C for 12 h. This process resulted in the Al-Si@$Al(OH)_3$ sample. Moreover, the Al-Si@$Al(OH)_3$ sample was prepared using the water bath method under the same conditions. With different amounts of Si and particle sizes, Al-Si powder was utilized to obtain different samples, as detailed in Table 1. The Al-Si powder, with 12 at. % of Si and a diameter of 75 µm, was labeled A17. The A17 sample was hydrothermally treated for 3 h to synthesize Al-12Si@$Al(OH)_3$, and the product was labeled Al-12Si@$Al(OH)_3$(H), abbreviated to A17H3; meanwhile, the Al-12Si@$Al(OH)_3$ synthesized by the water bath method for 3 h was labeled Al-12Si@$Al(OH)_3$(W), abbreviated to A17W3. The experimental parameters, i.e., reaction time, silicon content, and Al-Si particle diameter, were changed to investigate the influence of different parameters on the precursor microstructure.

Table 1. Parameters of the Al-Si powders.

Sample	Si Content/at. %	Mean Size/µm
Al-12Si(A17)	12	75
Al-20Si(A23)	20	38
Al-20Si(A27)	20	75
Al-30Si(A37)	30	75

The morphology of the as-prepared core–shell composite was observed using a scanning electron microscope (SEM, JEOL JSM-6700F, Japan). X-ray diffraction (XRD) analysis was carried out using the Rigaku D/MAX-2500 X-ray diffractometer (Japan) with a scan rate of 10 °/min. Fourier-transform infrared (FTIR) spectroscopy was conducted using a Nicolet-5700 instrument. The pore structure and BET surface area were tested at 77 K via N_2 adsorption/desorption isotherms.

3. Results and Discussion

3.1. Analysis of Samples

Figure 1 presents the XRD patterns of various precursors prepared by the water bath and hydrothermal methods. The characteristic peaks of Al and Si can be clearly observed; however, a weak peak of the bayerite phase ($Al(OH)_3$, PDF# 20-0011) was observed in the XRD pattern of A17W6, which is consistent with previous reports that bayerite is formed by the reaction of Al with water [25]. The characteristic peaks of the $Al(OH)_3$ phase in Figure 1c,d were too weak and could not be observed in the XRD pattern. To further illustrate the existence of the bayerite phase in the hydrothermally-prepared precursors, the FTIR spectrum of A17H6 is shown in Figure 2. The strong peak at 3435 cm^{-1} illustrates the existence of $Al(OH)_3$. Moreover, Al-O stretching vibrations were confirmed by the presence of peaks at 734 and 611 cm^{-1}, confirming the existence of $Al(OH)_3$ [25]. It has been reported that Si is essential to form boehmite [19], i.e., the $Al(OH)_3$ was successfully formed in all precursors.

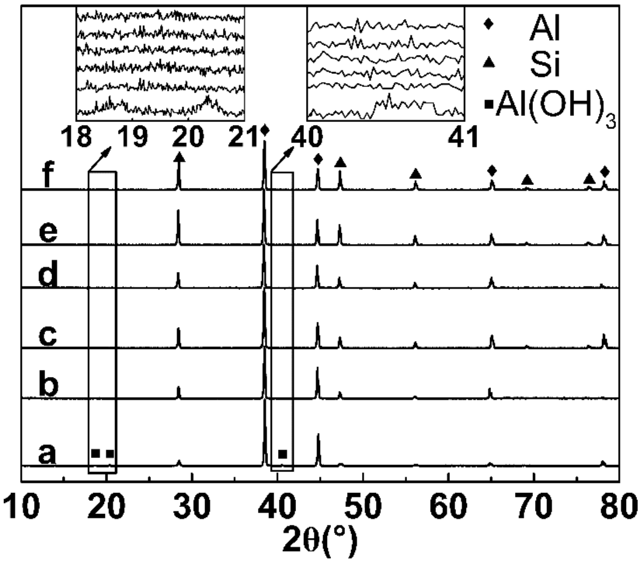

Figure 1. XRD patterns of the precursors: (**a**) A17W6, (**b**) A17H6, (**c**) A27W6, (**d**) A27H6, (**e**) A37W6, and (**f**) A37H6.

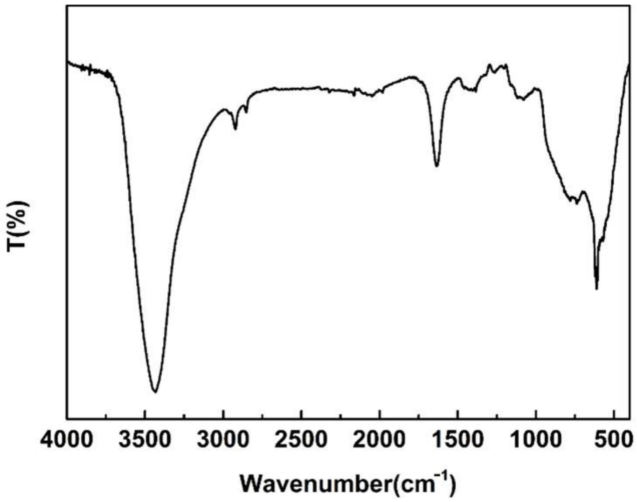

Figure 2. FTIR spectrum of A17H6.

Figure 3 presents the SEM images of A27 prepared using different methods and times. The thickness of the nanosheets prepared by the water bath method was thinner than those of the hydrothermal method. As shown in Figure 4a–c, the thickness of the nanosheets also increased with the increase in the reaction time. Moreover, the same conclusion can be obtained from Figure 4d–f. The growth of the nanosheets on the surface of Al-Si@$Al(OH)_3$(W) was abnormal, and abundant impurities appeared around the core–shell structure, decreasing the active sites and compromising the catalytic performance. Compared with the water bath method, the hydrothermal method is a better way to prepare pure Al-Si@$Al(OH)_3$. It is noteworthy that the increase in time only affected the thickness of the nanosheets, and we can decrease the hydrothermal time to obtain equally distributed core–shell structures, shortening the preparation cycle.

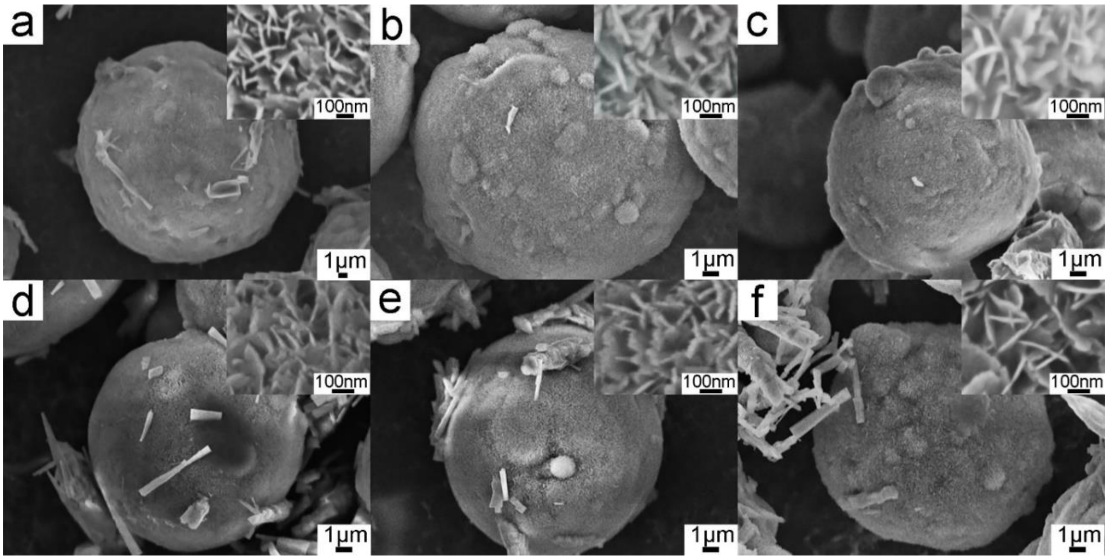

Figure 3. SEM images of the precursors: (**a**) A27H3, (**b**) A27H6, (**c**) A27H9, (**d**) A27W3, (**e**) A27W6, and (**f**) A27W9.

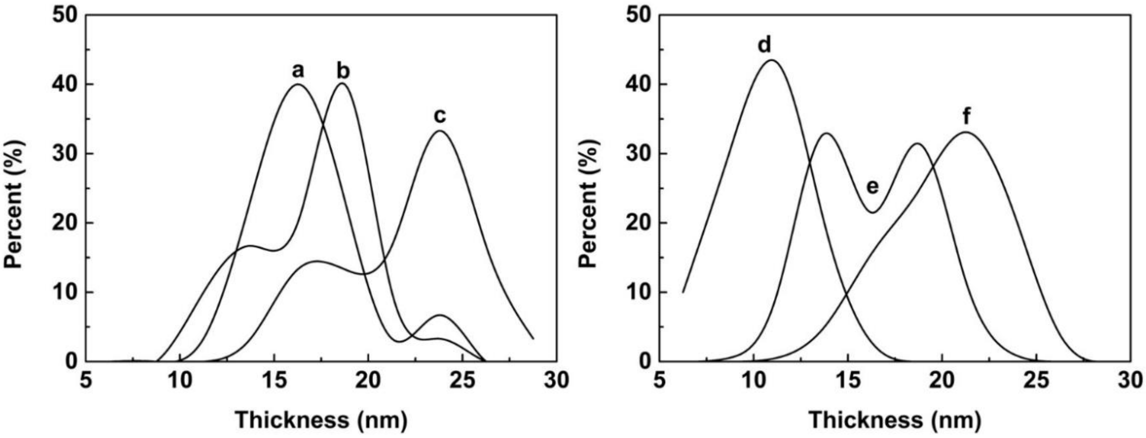

Figure 4. The thickness distribution of the $Al(OH)_3$ nanosheets: (**a**) A27H3, (**b**) A27H6, (**c**) A27H9, (**d**) A27W3, (**e**) A27W6, and (**f**) A27W9.

As shown in Figure 5, Al-Si@$Al(OH)_3$ can be synthesized using Al-Si powder with different amounts of Si. The thickness distribution of the nanosheets is shown in Figure 6. The thickness distribution of the A27H6 was more concentrated than the others, showing the influence of the Si morphology on the thickness uniformity of the $Al(OH)_3$ nanoflakes. It can be inferred that the distribution of $Al(OH)_3$ nanoflakes becomes more concentrated and the thickness tends to reduce with the increase in the Si content.

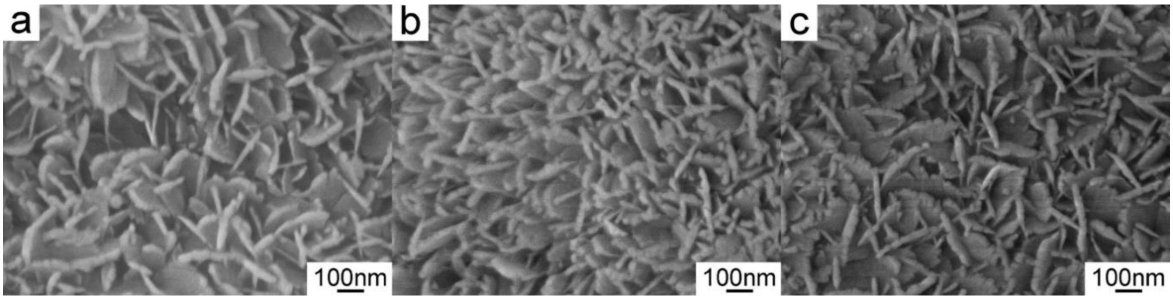

Figure 5. SEM images of (**a**) A17H6, (**b**) A27H6, and (**c**) A37H6.

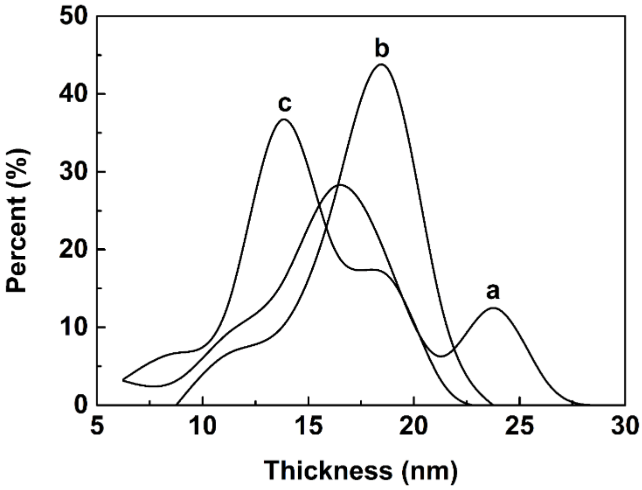

Figure 6. The thickness distribution of the $Al(OH)_3$ nanosheets: (**a**) A17H6, (**b**) A27H6, and (**c**) A37H6.

To further investigate the influence of the Al-Si particle size, two different grain sizes were utilized to form Al-20Si@$Al(OH)_3$(H). It is observed that there was a small distinction in the morphology and thickness distribution of the nanoflakes, as shown in Figure 7a,b and Figure 8a,b. As the particle size of the Al-Si powder influenced the Si morphology, the density of the primary Si on the surface of the Al-Si particles increased with the decrease in the mean particle size. It can be concluded that the particle size renders a negligible influence on the structure of the $Al(OH)_3$ nanoflakes. Figure 9a presents the adsorption/desorption isotherms of A27H6, which belonged to type-IV of IUPAC and indicated the presence of mesopores. The specific surface area was found to be 19.5573 m^2/g, which indicates that the nanoflakes increased the specific surface area of the Al-Si particles. The pore diameter of A27H6 was mainly distributed below 25 nm, as shown in Figure 9b.

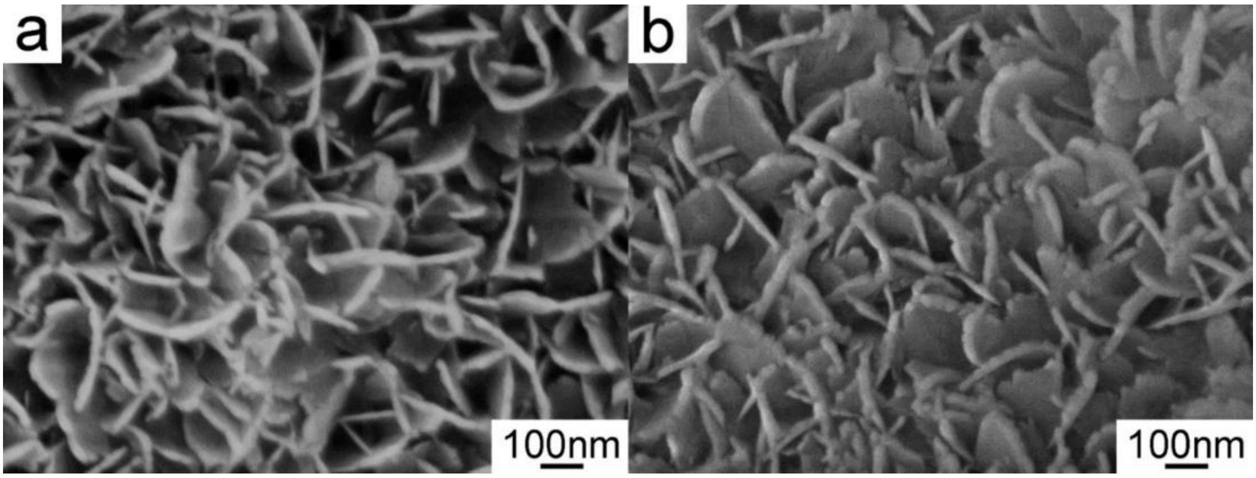

Figure 7. Surface morphologies of (**a**) A23H6 and (**b**) A27H6.

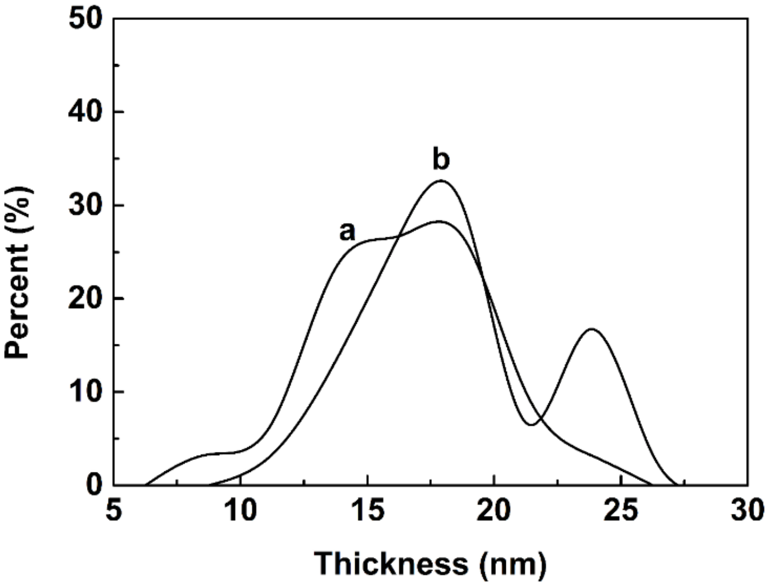

Figure 8. Thickness distribution of the $Al(OH)_3$ nanosheets: (**a**) A23H6 and (**b**) A27H6.

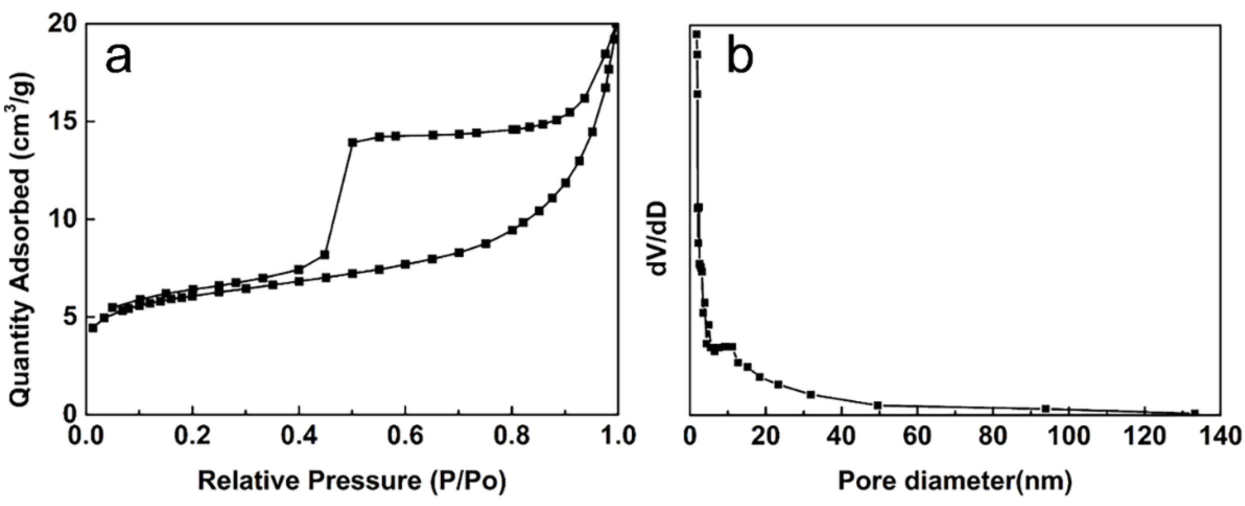

Figure 9. The A27H6 (**a**) adsorption/desorption isotherms and (**b**) pore size distribution.

3.2. Impact of Silicon Morphology

In order to reveal the growth mechanism during the initial stage, the ground and polished Al-20Si alloy was treated with deionized water at 80 °C for 30 min, and morphological changes were observed, as shown in Figure 10. Overall, the distribution of nanoflakes was mainly focused on the interphase between the Si phase and the Al matrix, which indicates that the nucleation of $Al(OH)_3$ mainly occurred at the Al/Si interphase, and the nanosheets completely covered the surface of the Al-Si particle with the increase in the reaction time. In addition, more nanosheets were observed on the surface of the eutectic Si than the primary Si phase, which indicates the influence of the Si area on the $Al(OH)_3$ deposition.

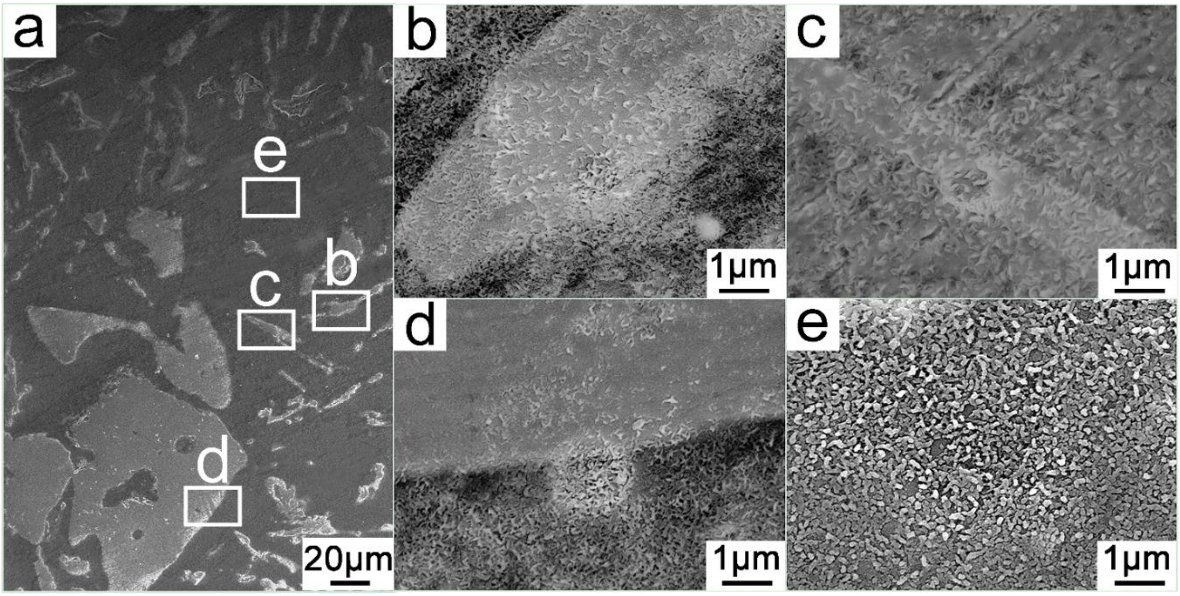

Figure 10. The morphology of the Al-20Si@Al$(OH)_3$(W): (**a**) Al-20Si, (**b**,**c**) eutectic silicon, (**d**) primary silicon, and (**e**) aluminum.

4. Conclusions

In summary, the influence of the Si content and Al/Si particle size on the morphology and thickness of the Al$(OH)_3$ nanosheets was systematically investigated. The main conclusions are as follows:

1. The comparison of the microstructure between the hydrothermal and water bath methods revealed that the hydrothermal method was a better way to prepare the Al-Si@Al$(OH)_3$ nanosheets than the water bath method. Overall, the reaction time rendered little effect on the structure of the Al-Si@Al$(OH)_3$ nanosheets.
2. The SEM images and pore size analysis demonstrated that the average thickness of the nanoflakes decreased with the increase in the Si content. Moreover, the distribution density of the Al$(OH)_3$ nanosheets remained constant when the mean particle size of Al-Si exceeded 38 μm.
3. The nucleation site of the Al$(OH)_3$ nanoflakes was on the interface between the silicon and the aluminum matrix in the initial stage. Relative to the area of the eutectic Si and Al matrix, the area of the primary Si was finally covered by the Al$(OH)_3$ nanosheets.

These results demonstrate that the preparation time of Al-Si@Al_2O_3 can be effectively reduced by regulating the Si content and average particle size of the Al-Si alloy. The current study offers an efficient strategy to synthesize an Al-Si@Al_2O_3 core–shell structure for a wide array of applications.

Author Contributions: Investigation, writing original draft and writing review & editing, Y.L.; investigation, P.C.; methodology, Y.W.; Formal analysis, methodology and resources, C.L.; All authors have read and agreed to the published version of the manuscript.

Funding: This work is supported by the Science and Technology Project of State Grid Corporation of China (Wei He SGZJ0000KXJS1900221) and the National Natural Science Foundation of China (Mei Zhao Grant No. 51672145).

Conflicts of Interest: The authors declare that they have no competing interests.

Abbreviations

SEM: Scanning electron microscope; FTIR: Fourier-transform infrared; IUPAC: International Union of Pure and Applied Chemistry.

References

1. Singh, R.; Bhateria, R. Core-shell nanostructures: A simplest two-component system with enhanced properties and multiple applications. *Environ. Geochem. Health* **2020**, *43*, 2459–2482. [CrossRef]
2. Chang, Y.C.; Lin, Y.W. MoS_2@SnO_2 core-shell sub-microspheres for high efficient visible-light photodegradation and photocatalytic hydrogen production. *Mater. Res. Bull.* **2020**, *129*, 110912. [CrossRef]
3. Zou, Q.C.; Jie, J.C.; Shen, Z.F.; Han, N.; Li, T.J. A new concept of Al-Si alloy with core-shell structure as phase change materials for thermal energy storage. *Mater. Lett.* **2019**, *237*, 193–196. [CrossRef]
4. Liu, X.M.; Niu, C.G.; Zhen, X.P.; Wang, J.D.; Su, X.T. Novel approach for synthesis of boehmite nanostructures and their conversion to aluminum oxide nanostructures for remove Congo red. *J. Colloid Interface Sci.* **2015**, *452*, 116–125. [CrossRef]
5. Wang, Y.P.; Hao, X.Q.; Wang, G.R.; Jin, Z.L. Rational design of a core–shell-shaped flowerlike $Mn_{0.05}Cd_{0.95}S$@NiAl-LDH structure for efficient hydrogen evolution. *Catal. Lett.* **2021**, *151*, 634–647. [CrossRef]
6. Li, G.X.; Wu, C.; Dong, P.; Ji, D.; Zhang, Y.F. Core–Shell HZSM-5@silicalite-1 composite: Controllable synthesis and catalytic performance in alkylation of toluene with methanol. *Catal. Lett.* **2020**, *150*, 1923–1931. [CrossRef]
7. Yang, L.Q.; Liu, Y.L.; Wang, L.; Zhao, Z.J.; Xing, C.J.; Shi, S.H.; Yuan, M.L.; Ge, Z.M.; Cai, Z.Y. $Co_{5.47}N$/rGO@NF as a high-performance bifunctional catalyst for urea-assisted hydrogen evolution. *Catal. Lett.* **2019**, *149*, 3111–3118. [CrossRef]
8. Xie, C.; Zhao, Y.B.; Song, Y.X.; Liu, Y.J.; Wang, Y.Y.; Yang, P. Effect of cores on photoluminescence of hybrid SiO_2-coated CdTe quantum dots. *J. Nanosci. Nanotechnol.* **2020**, *20*, 5478–5485. [CrossRef]
9. Yao, C.L.; Zhu, J.M. Synthesis, characterization and photocatalytic activity of Au/SiO_2@TiO_2 core-shell microspheres. *J. Braz. Chem. Soc.* **2020**, *31*, 589–596. [CrossRef]
10. Gandomi, F.; Sobhani-Nasab, A.; Pourmasoud, S.; Eghbali-Arani, M.; Rahimi-Nasrabadi, M. Synthesis of novel Fe_3O_4@SiO_2@Er_2TiO_5 superparamagnetic core–shell and evaluation of their photocatalytic capacity. *J. Mater. Sci. Mater. Electron.* **2020**, *31*, 10553–10563. [CrossRef]
11. Han, D.D.; Xiao, N.R.; Liu, B.; Song, G.X.; Ding, J. One-pot synthesis of core/shell-structured NiS@onion-like carbon nanocapsule as a high-performance anode material for Lithium-ion batteries. *Mater. Lett.* **2017**, *196*, 119–122. [CrossRef]
12. Li, S.T.; Shi, G.M.; Liang, J.S.; Dong, X.L.; Shi, F.N.; Yang, L.M.; Lv, S.H. Core-shell structured Co@CN nanocomposites as highly efficient dual function catalysts for reduction of toxic contaminants and hydrogen evolution reaction. *Nanotechnology* **2019**, *31*, 065701. [CrossRef]
13. Quan, F.; Wu, Q.H.; Mao, A.Q.; Zuo, D.S.; Wang, B.; Yu, H.Y. Cu/Ag core/shell particles via modified arc discharge method. *Int. J. Mater. Res.* **2018**, *109*, 270–272. [CrossRef]
14. Ren, Y.Y.; Yang, X.J.; Li, L.L.; Li, C.L.; Zhang, X.H.; Lu, Z.M.; Yu, X.F. Pd@Pt core–shell nanoflowers as efficient catalyst toward methanol oxidation. *Catal. Lett.* **2020**, *150*, 3415–3423. [CrossRef]
15. Wang, Z.T. Cycloaddition of propargylic amines and CO_2 by Ni@Pd nanoclusters confined within metal–organic framework cavities in aqueous solution. *Catal. Lett.* **2020**, *150*, 2352–2364. [CrossRef]
16. Zhang, X.T.; He, N.; Liu, C.Y.; Guo, H.C. Pt–Cu alloy nanoparticles encapsulated in silicalite-1 molecular sieve: Coke-resistant catalyst for alkane dehydrogenation. *Catal. Lett.* **2019**, *149*, 974–984. [CrossRef]
17. He, F.; Sui, C.; He, X.D.; Li, M.W. Comparison of structure and phase change characteristic of microencapsulated core/shell Al–Si alloy microparticles synthesized by two methods. *J. Sol-Gel Sci. Technol.* **2015**, *76*, 1–10. [CrossRef]
18. Daraio, D.; Villoria, J.; Ingram, A.; Alexiadis, A.; Stitt, E.H.; Munnoch, A.L.; Marigo, M. Using Discrete Element method (DEM) simulations to reveal the differences in the γ-Al_2O_3 to α-Al_2O_3 mechanically induced phase transformation between a planetary ball mill and an attritor mill. *Miner. Eng.* **2020**, *155*, 106374. [CrossRef]
19. Liu, G.G.; Ye, H.Q.; Dai, Y.N.; Yu, L.Y.; Jiang, H.; Zhou, Y.H.; Han, K. A facile method for in situ growing nano-flaky γ-Al_2O_3 on the surface of Al–Si alloy sphere. *J. Alloys Compd.* **2015**, *647*, 18–23. [CrossRef]
20. Dai, Y.N.; Liu, G.G.; LI, W.; Han, K.; Zhou, Y.H.; Ye, H.Q. Preparation and catalytic application Al-Si@Al_2O_3 core-shell structured carrier. *Nonferrous Met. Sci. Eng.* **2016**, *7*, 42–48.
21. Hearn, W.; Bogno, A.A.; Spinelli, J.; Valloton, J.; Henein, H. Microstructure Solidification Maps for Al-10 Wt Pct Si Alloys. *Metall. Mater. Trans. A* **2019**, *50*, 1333–1345. [CrossRef]
22. Cai, Z.Y.; Zhang, C.; Wang, R.C.; Peng, C.; Qiu, K.; Wang, N.G. Effect of solidification rate on the coarsening behavior of precipitate in rapidly solidified Al-Si alloy. *Prog. Nat. Sci. Mater. Int.* **2016**, *26*, 391–397. [CrossRef]
23. Cai, Z.Y.; Zhang, C.; Wang, R.C.; Peng, C.Q.; Wu, X.; Li, H.P.; Yang, M. Improvement of deformation capacity of gas-atomized hypereutectic Al-Si alloy powder by annealing treatment. *Trans. Nonferrous Met. Soc. China* **2018**, *28*, 1475–1483. [CrossRef]
24. Cai, Z.Y.; Wang, R.C.; Zhang, C.; Peng, C.Q.; Xie, L.C.; Wang, L.Q. Characterization of rapidly solidified al-27 si hypereutectic alloy: Effect of solidification condition. *J. Mater. Eng. Perform.* **2015**, *24*, 1226–1236. [CrossRef]
25. Godart, P.; Fischman, J.; Seto, K.; Hart, D. Hydrogen production from aluminum-water reactions subject to varied pressures and temperatures. *Int. J. Hydrogen Energy* **2019**, *44*, 11448–11458. [CrossRef]